The Oil Industry, it Space Transformations and Impacts in the Thermal Field of the City of Macaé, in the State of the Rio de Janeiro /Brazil

A Indústria do Petróleo, suas Transformações Espaciais e seus
Impactos no Campo Térmico da Cidade de Macaé, no Estado do Rio de Janeiro/Brasil

Paloma Arantes Wilson[1]; José Ricardo de Almeida França[1];
Andrews José de Lucena[2] & Vitor Fonseca Vieira Vasconcelos de Miranda[1]

[1]Universidade Federal do Rio de Janeiro, Instituto de Geociências, Departamento de Meteorologia,
Campus Universitário da Ilha do Fundão, Av. Athos da Silveira Ramos 274, Bl. H, Cidade Universitária
Ilha do Fundão, 21941-916, Rio de Janeiro, RJ, Brasil
[2]Universidade Federal Rural do Rio de Janeiro, Instituto de Agronomia, Departamento de Geografia,
Campus Sede Seropédica, BR-465, Km 7, 23897-000, Seropédica, RJ, Brasil
E-mails: paloma_arantes@hotmail.com; jricardo@igeo.ufrj.br; lucenageo@gmail.com; vitormiranda91@yahoo.com.br

Resumo

Este trabalho analisa o padrão espacial e temporal da Temperatura da Superfície Continental (TSC) na cidade de Macaé, baseado no Índice de Vegetação por Diferença Normalizada (NDVI) e no uso e cobertura do solo. As análises foram realizadas pelas imagens do sensor Thematic Mapper (TM), a bordo do satélite Landsat 5. Os mapas da TSC e NDVI foram gerados por meio de programas de sensoriamento remoto. Mapas para uso e cobertura do solo também foram gerados para dias específicos em 1980, 1990, 2000 e 2010, o que possibilitou uma análise temporal, espacial e sazonal. Os resultados mostraram que, com o crescimento da área urbana de Macaé, houve pontos favoráveis à formação de ilhas de calor, mostrando que as áreas construídas encontram-se mais aquecidas do que anteriormente.
Palavras-chave: Temperatura da Superfície Continental; Índice de Vegetação por Diferença Normalizada; Ilha de calor Urbana

Abstract

This work analyzes the spatial and temporal pattern of Land Surface Temperature (TSC) in the urban area of Macaé, based on Normalized Difference Vegetation Index (NDVI) and use and land cover. Analyses were performed by Thematic Mapper (TM) sensor images, aboard the Landsat 5. TSC and NDVI maps were generated through remote sensing data. Maps for use and land cover were also generated for specific days in 1980, 1990, 2000 and 2010, which enabled a spatial and seasonal temporal analysis. The results showed that, with the growth of the urban area of Macaé, there were points favorable to the formation of heat islands, showing that the built-up areas are warmer than in the past.
Keywords: Land Surface Temperature; Normalized Difference Vegetation Index; Urban Heat Island

1 Introduction

The urban's space production in Brazil was intensified after 1940, deeply connecting it with the industrialization process in the country. The urbanization has not only transformed the importance of the large and middle cities, but also their morphological structures. This urbanization is also producing and creating infrastructure, better service and sanitation conditions in addition, it has impacted the social and environmental implications, such as the atmospheric pollution and growth of unhealthy dwellings, like the slums.

One of the results of the urban nucleus's growth is the installation of the industrial complexes. The environmental impacts promoted by the industries are not prerogatives of Brazil, since, European countries know similar problems, but they look for initiatives that conjugate quality of life and economic growth. There is a scale of problems attributed to the environmental impacts caused by industrial complexes: resonant pollution, pollution of waters, of the ground, of the air, etc. The chemical industries, especially those of oil, have been a major cause of environmental problems, when pollutant gases and particulate matter are released into the atmosphere, besides the leak and eviction of oils in the oceans (Leal *et al.*, 2008).

The installation of an industry in small and medium-sized cities can modify the social and economic routine. Some cities in the state of Rio de Janeiro have assumed new characteristics (socioenvironmental) after an implantation of industries. The case of Macaé, a county in the northern region of the state of Rio de Janeiro, fits this situation. Because of the oil installation in the Macaé, the city's population increased considerably in the last two decades growth represents the greatest geometric growth rate in all of Brazil between 2000 and 2010 (125%) as transformations conducted by the industry can cause environmental impact of different magnitudes, including in the local urban climate.

An area of the city with high concentration of heat sources becomes favorable to the formation urban heat island. The urban heat island is a product of the urban climate (Oke, 1987) and is related to the climate's urban impacts, resulting from intense urbanization. Changes in surface cover change the flow of energy due to the thermal absorption capacity of the building materials used in the city. Thus, the point of the city that concentrates materials with thermal characteristics of high heat conduction (buildings, asphalt, population density, etc) presents greater thermal contrasts when compared to the points of the city with vegetated areas and less inhabited areas.

The surface of the urban centers can provide the formation of the heat island through little spaced constructions that reduces the loss of radiative heat - mainly in the nocturnal period. The construction's roofs that decrease convective heat loss from the surface and close to the surface. The surface's thermal properties present a larger thermal surface, containing and supporting more heat.

Remote sensing is one of the most successful automatic data collection technologies for surveying and monitoring terrestrial resources on a global scale. With a wide area of application, remote sensing has been widely used in urban climate studies, including the assessment of urban heat island from thermal bands Rao (1972) was the pioneer using sensors to monitor the urban climate. This author mapped the surface temperature of cities along the mid-Atlantic coast from the TIROS 1 (Television IR Operational Satellite) thermal band (102-125 um) In the 1970s, Calrson *et al.* (1977) and Matson *et al.* (1978) used thermal data from the AVHRR sensor to map the heat island. The first authors analyzed the temperature of the daytime surface in Los Angeles and found a greater gradient in the industrial and central areas compared to the vegetated areas Similarly, Matson *et al.* (1978) found higher temperatures in the industrial areas of the Midwest region of the USA.

Studies on urban heat island using remote sensing have been conducted for different cities in the world: Shenzhen, China (Chen *et al.*, 2012); Casablanca, Morocco (Rhinane *et al.*, 2012); Madrid, Spain (Sobrino *et al.*, 2012); Shanghai, China (Li *et al.*, 2011); Bucharest, Romania (Cheval *et al.*, 2009); Arizona, USA (Buyantuyev & Wu, 2010); Rio de Janeiro, Brazil (Lucena *et al.*, 2013; Sena *et al.*, 2014; Sena *et al.*, 2014; Peres *et al.*, 2018), among others.

In this context, the objective of this work is to perform a time-space analysis of the expansion of the urban area of the city of Macaé and its environs caused by the oil industry and the continental surface temperature (LST) in the last 30 years. The purpose is to identify possible favorable areas to the occurrence of the urban heat island.

2 Study Area and Material
2.1 Study Area

The city of Macaé is located in the state of Rio de Janeiro's northern sector of heterogeneous landscape. This area combines oceanic mountains with one of the few areas of preserved Atlantic forest. The area that will be analyzed in this study does not include all municipal boundaries of Macaé, but rather the most urbanized area and its immediate surroundings (Figure 1).

Due to sugar cane cultivation, coffee and fishing, Macaé city was essentially agricultural until the middle of the 20th century. Since 1974, with the discovery of oil in the Campos Basin and the establishment of Petrobras, the city has taken a new form, mainly in the economic and social sphere (Marques, 2008). Accelerated population growth has been linked to the expansion of the urban network of services, infrastructure and new land uses. The population increased with the expansion of housing development areas, and the labor force was mainly absorbed by the oil and gas sector.

According to data from Brazilian Institute of Geography and Statistics (IBGE, 2019), the Macaé population increased from 74.000 inhabitants in 1974 to 206.728 in 2010 and 251.631 inhabitants estimated in 2018. The urban population accounted for by the 2010 census (IBGE, 2019) is 202.873 inhabitants, corresponding to 98% of the total population, while the rural population is 3.875 inhabitants (19%).

The urban and rural population's evolution, between the 1960s and 2010, highlights the marked decline of the rural population and the predominance of the urban. The population density also increased significantly, from 2628 inhabitants / km² in 1960 to 1699 inhabitants / km² in 2010.

Macaé's physical aspects are marked by heterogeneous features in relation to relief and vegetation. Macaé covers areas of river and marine plains in the portion closest to the ocean and areas of steeper slope represented by hills, isolated hills and steep hills. There is a 40 km stretch of beaches opposite of a mountainous region with rivers and waterfalls. The altitude increases from the coastal strip to the foothills of the Serra do Mar.

Figure 1 Location of the city of Macaé in the state of Rio de Janeiro, Brazil.
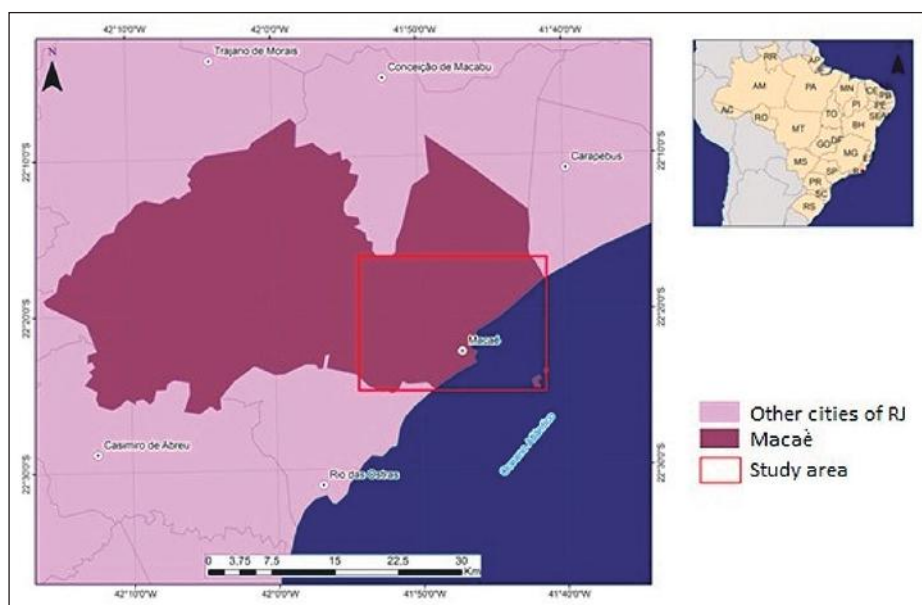
2.2 Data Source

In order to fulfill the objective, images of the Thematic Mapper (TM) sensors, present in Landsat 5 satellite, were used. The following products were generated: Land Surface Temperature (LST) and Normalized Difference Vegetation Index (NDVI), which will be discussed below.

The TM sensor, as well as the ETM + (aboard on the Landsat 7), has the band 6 within the atmospheric window (range between 8 and 14 μm, transparent to the long wavelength release to the space by the terrestrial surface), thus being the thermal infrared region. This makes it suitable for the mapping of the LST (temperature of the objects in the surface, present in the image).

In this analysis, six images were selected between the period from 1985 to 2010 (03/23/1985; 01/09/2005; 03/23/2010; 07/30/1991; 07/04/2005; 09/04/2010 - the images of the month 01 and 03 represent the wet period; the images of the month 07 and 09 represent the dry period, orbit-point 216/75 corresponding to the daytime period (between 12h and 13h, UTC). The images chosen were in accordance with the following criteria: absence of clouds and radiometric quality. One of the greatest difficulties in selecting the images was in relation to the presence of clouds, because, for many dates previously proposed, the presence of clouds exceeded 20%, especially in the continental portion of the images. As a result, images with less than 20% cloud coverage were prioritized regarding the radiometric quality, the presence of noises that may prevent image processing, a selection was made based on the visual criterion and also on the analysis of the non-realistic physical values.

For each decade, one image was obtained. Since not enough images were found to observe a pattern of behavior, mainly for the analysis of LST, the selected images will be considered as episodes that may represent minimally the last decades. The images obtained were: 03/23/1985, 07/30/1991, 01/09/2005, 03/23/2010, which will be considered from the 1980s, 1990, 2000 and 2010 decade, respectively. The seasonal analysis, will be done only for the LST, images were obtained from 07/04/2005

and 09/04/2010. Six maps were generated for the LST analysis, 4 land use and land cover maps, 4 maps for NDVI 4 maps with integrated LST analysis and land use and coverage

3. Methods
3.1 Selecting and Processing Images

After selecting images with lower cloud coverage and better radiometric quality, images were georeferenced, cropped and re-sampled with ENVI software, based on an RGB image of Landsat 5, corresponding to the date of 09/23/1988. The georeferencing took into account 10 points, which were selected with the base image and reproduced in the others, with a general error less than 0.3. The image cut-out (Figure 1) was performed in the desired area - an area encompassing an urbanized region of Macaé and its non-urbanized surroundings. Subsequently, the same clipping was used as a basis for cropping. The resampling process takes into account the number of lines and columns of the bands (with spatial resolution of 30 m of 120 m), and was done computing a correction factor: Xfac and Yfac, dividing the number of lines and columns (ie: Yfac = 130/120 and Xfac = c30/c120, where L is the number of lines and C is the number of columns).

After georeferencing, cropping and resampling, geotiff formatted "gribs" files were used to prepare land use maps of LST and NDVI. MATLAB software was used to convert digital values (DV) into radiance, reflectance, brightness temperature and for the masking of clouds and ocean. In order to perform this transformation it was necessary to apply the equation and calibration constants, according to Chander & Markham (2003) and Chander *et al*. (2009), carried out in the works of Lucena *et al*. (2013) and Peres *et al*. (2018). To know the radiant's value of energy that arrives at the sensor, it's necessary to convert the digital values (DV), and that can be done with the Equation 1:

$$L_i = \left(\frac{LMAX_i - LMIN_i}{Qcal_{max}} \right) Qcal + LMINi \quad (1)$$

L_i is the spectral radiance in the channel i in Wm^{-2}sr^{-1}μm^{-1}; LMAXi is the maximum radiance value in the band i in Wm^{-2} sr^{-1}μm^{-1}; LMIN$_i$ is the minimum radiance value in the band i in Wm^{-2} sr^{-1}μm^{-1}; Qcal is the value of the digital number (DV); Qcalmax is the maximum value of DV.

After transforming the DV into radiance value, it was necessary to find the reflectance value. In order to transform the radiance into reflectance it is necessary to adopt different calculations for the non thermal infrared channels (1, 2, 3, 4, 5 and 7) in relation to the thermal infrared channel (6). Thus, through Equation 2 we can find the reflectance for the non thermal infrared channels:

$$\rho_t = \frac{\pi * L_t * d^2}{ESUN_t * COS\theta_s} \tag{2}$$

t is the reflectance in the channel t; d is the distance Earth-Sun in astronomical units; $ESUN_t$ is the mean value of solar irradiance in channel t in $Wm^{-2}\mu m^{-1}$; and θ_s is the solar zenith angle. For channel 6, the radiance needs to be transformed to brightness temperature (Tb) through the inverse Planck function (Bi (Tb)):

$$Tb = \frac{K_2}{\ln\left(\frac{K_1}{L_t}+1\right)} \tag{3}$$

Tb is the brightness temperature in Kelvin (K); K_1 and K_2 are the Landsat calibration constants 1 and 2 in $Wm^{-2} sr^{-1} \mu m^{-1}$, where the K_1 = 60776 (Landsat 5), and the K_2 = 126056 (Landsat 5); and L is the radiance.

3.2 Use Map Generation and Land Cover

In order to map the land use and cover, a process of vectoring the images in the 1: 30.000 scale was carried out, with projection in UTM WGS 84 24 S, due to resolution and correspondence of Landsat 5 images. The maps were elaborated from the images from those dates that represent the decades (1980s, 1990s, 2000s and 2010s, respectively). The defined classes were: urban high density, urban medium density, urban low density, flooded area, vegetation and water. The urban class was differentiated in high and low because of the interest in the evolution of the urban area of the region.

The images' classifying method is automatic (some polygons are identified and classified to relate later to the other areas) for areas considered as vegetation, and not supervised (they were classified according to the polygons size and infrastructure's density) for urban areas. In addition to manual vectoring, comparisons with Google Earth images were of great importance. The classification's choice method should consider different factors, among them, the image's spatial resolution, and Landsat presents medium resolution, which may generate spectral confusion among some classes. The best response for classification for the urban area was the unsupervised method (manual vectoring), performed in Esri's Arcgis 10.1 software. The polygons generated for the urban class will facilitate LST analysis, as they may be cross-referenced in a single image.

3.3 Clouds and Ocean Masking

Most of the images available through the database at orbit-point 216/75 show cloud coverage above 20%. Cloud cover influences the emitted thermal radiation and reflected solar radiation, which can prevent the identification of pixels, causing an error in the estimation of surface parameters. To ensure that the images were totally cloud free, three cloud covering methods were used (França & Cracknell, 1995; Chen *et al.*, 2002)

The first one is the reflectance value threshold technique, which is based on a threshold of 0.3 (for the reflectance in Landsat band 3 around 0.6 μm), where has been determined that any pixel which has a reflectance value greater than 0.3 is considered to be covered by a cloud.

The second one is the Gross Threshold technique, where the cloud-covered pixel was classified through the brightness temperature of channel 6. A threshold of less than or equal to 278 K was chosen. That is related to the temperature variation in equatorial climate, which is small.

The last one is the Q-technique, where an equation with the ratio of Landsat channel 3 (visible red) and 4 (near infrared) reflectance, ie Q=ρ4/ρ3, is applied. The values assigned to Q on the cloud-covered pixel are approximately equal to 10, since there is a similar effect of reflected energy scattering for both channels. There is a difference between the value of Q for the continental surface and for the sea surface: in the mainland and in vegetated areas the

value of Q is generally higher than 10, because of the higher reflectance values in band 4 in relation to 3. While on the sea surface, ρ_3 it is much larger than ρ_4 because of the near-infrared absorption effect by the water. Once the technique was applied to the continent and to the sea surface, it was determined that for the values of Q greater than or equal to 0.8 and less than or equal to 1.6 the pixel will be classified as a cloud. When Q is less than 0.8 the pixel was classified as water, and when it is greater than 1.6, surface land.

3.4 Land Surface Temperature (LST)

The Land Surface Temperature (LST) was retrieved using data from Landsat 5, with band 6, the only channel of the TM sensor in the thermal infrared spectral range (Lucena *et al.*, 2013; Peres *et al.*, 2018). Different methods were proposed to correct atmospheric effects on LST (Souza & Silva, 2005). The method used here was the same one adopted by Lucena *et al.* (2013) and Peres *et al.* (2018). Equation 4 was used to retrieve LST.

$$T_S = T_b + \Delta T \qquad (4)$$

T_s is LST in Kelvin (K), T_b is the brightness temperature in band 6, obtained according to Equation 6; It is also the correction factor that makes the estimation of LST possible from the brightness temperature in band 6, given by:

$$\Delta T = \frac{B_t(T_b)\left(\frac{1}{\alpha_1}-1\right)-\frac{\alpha_2}{\alpha_1}B_t(T_a)}{\frac{\partial B_t(T_b)}{\partial T_b}} \qquad (5)$$

$$\propto_1 = \tau_t \varepsilon_t \qquad (6)$$

$$\propto_2 = (1 - \tau_1)[1 + (1 - \varepsilon_t)\tau_t] \qquad (7)$$

According to the above equations (from 4 to 7), to obtain LST, it is necessary to know the atmospheric parameters, such as: atmospheric transmittance (, the average temperature of the atmospheric layer (T_a), besides the emissivity of the continental surface (. T_a can be obtained through the following equation (Qin *et al.*, 2001):

$$T_a = 19,73 + 0,909T_0 \qquad (9)$$

T_0 is the air temperature at 2 m from the surface. The atmospheric transmittance was calculated based on the empirical relation of Souza & Silva (2005)

$$\tau_1 = 0,951 - 0,01 \cdot w \cdot \exp\left(\frac{3w}{1+w}\right) \qquad (10)$$

W is the water vapor content in g, acquired by the Leckner equation (Iqbal, 1983)

$$W = 0,493 \, UR \cdot \frac{e_s}{T_0} \qquad (11)$$

where UR is the relative humidity and *s* e is the saturation pressure of water vapor in hPa, based on equation (Iqbal, 1983):

$$e_s = 0,01\exp\left(26,23 - \frac{5416}{T_0}\right) \qquad (12)$$

It is still necessary to know the emissivity value of the surface to obtain the LST, and since the sensor used in this study (TM) has a single thermal channel, a relation between the surface emissivity and the leaf area index LAI according to Bastiaanssen (2000). The LAI is a biomass indicator that makes it possible to estimate the density of the vegetated canopy (Allen *et al.*, 2002), and can be obtained as a function of SAVI (Soil Adjusted Vegetation Index). SAVI is an index that seeks to mitigate the effect or characteristics of the soil surface on the final result of the vegetation index. With this, the SAVI, the LAI and then the emissivity were obtained from the following equations:

$$SAVI = (1 + L)(\rho 4 - \rho 3)/(L + \rho 4 + \rho 3) \qquad (13)$$

$$IAF = -\frac{\ln\left(\frac{0,69 - SAVI_{ID}}{0,59}\right)}{0,91} \qquad (14)$$

$SAVI_{ID}$ = SAVI calculated with L=01

$$\varepsilon_t = 0,97 + 0,0033 * LAI \qquad (15)$$

3.5. Normalized Difference Vegetation Index - NDVI

The NDVI is an index widely used in urban climate analysis, since it allows the identification of the vegetation state present in an area, and can be correlated with the urban expansion and the local LST variation (Julien et al., 2006). The NDVI can be obtained through the following equation (Huete *et al*., 2002):

$$NDVI = \frac{\rho_4 - \rho_3}{\rho_4 + \rho_3} \qquad (16)$$

The vegetation has high reflectance in the near infrared region due to its cellular structure, and a low reflectance in the visible region associated to the energy absorption that is used in the process of photosynthesis. Thus, the higher the density of the vegetation cover, lower is the reflectance in the visible, and the greater in the near infrared (Ponzoni & Shimabukuro, 2007) NDVI values for vegetated areas vary between 03 and 10, where the highest values will be associated to the more vegetated vegetation cover. When values are below 0.6, vegetation presents stress characteristics, whereas values above 0.6, vegetation is represented as healthy (Huete *et al.*, 2002). For urbanized areas and exposed soil, the reflectance is similar with values close to zero,

3.6. Identification of Favorable Areas to the Urban Heat Island (UHI)

To identify areas favorable to the heat island, the hottest points will be analyzed. Both of the same time period and location similarly, areas classified as "urban" (high, medium or low) and those not considered as urban will be correlated to hot spots. The analysis of LST is based on the variation of NDVI, since these can better represent the urban expansion and changes in land use and cover that can lead to a change in the LST. Such analysis is due to the facts: the values obtained of LST are of at most 2 images per decade, which does not, in fact, represent the local temperature pattern; were not considered atmospheric phenomena that would be making the image period warmer or colder than normal.

4. Results and Discussion
4.1 The Land Use and Land Cover Time-Space Analysis

Between the 1980s and 1990s, the "medium--density urban" class expanded towards the north coast, and in the vicinity of the Imboassica lagoon, and the "medium-density urban" area had a relative advance towards the continent (Figure 2). The population of Macaé increased from 75.851 to 100.875 thousand inhabitants from 1980 to 1991, respectively.

The Maps of 1985 (Figure 2A) and 1991 (Figure 2B) have the same classification for the vegetation map. The vegetation class was defined as any green area identified according to the pixel recognition, besides the delimitation made by polygons of green areas visible to the eye. Only one class was defined for vegetation.

The greatest growth of the urbanized area was identified in the 2000s (Figure 3A), with a notable expansion of the built area, which extended parallel to the coast and towards the interior of the continent. Areas that were formerly considered as "medium density urban" changed very fast into the "high density urban" category, because the polygons considered in this area have spread, and buildings have become denser. From 1991 to 2000, the population increased from 100.875 to 132.461 thousand inhabitants.

The "dense urban" class extended even further in the period between 2005 and 2010 (Figure 3B). Areas previously classified as "medium density" were more occupied, making their buildings denser (in both buildings and population). At the moment, the population of Macaé increased from 132.461 to 206.728 thousand inhabitants, between 2000 and 2010, respectively.

The urban areas were delimited through polygons where any type of construction was observed. In areas where buildings were really close to each other or where it could be identified as the city, it was determined as a "high density urban" area. Likewise, where areas with fewer agglomerates were identified, they were identified as medium or low density.

The "vegetation" class was modified as the urban expansion occurred, remaining practically unchanged within the study area. It should be noted that some differences in terrain were not highlighted in the vegetation classification, such as rock outcrop area, sandy soils, undergrowth and pasture. Thus, for the LST results, and the NDVI index, these areas were identified with values peculiar for a vegetation.

The class "area susceptible to flooding" has undergone major changes. In the 1980s and 1990s flooded areas occupied a large area of the Macaé's
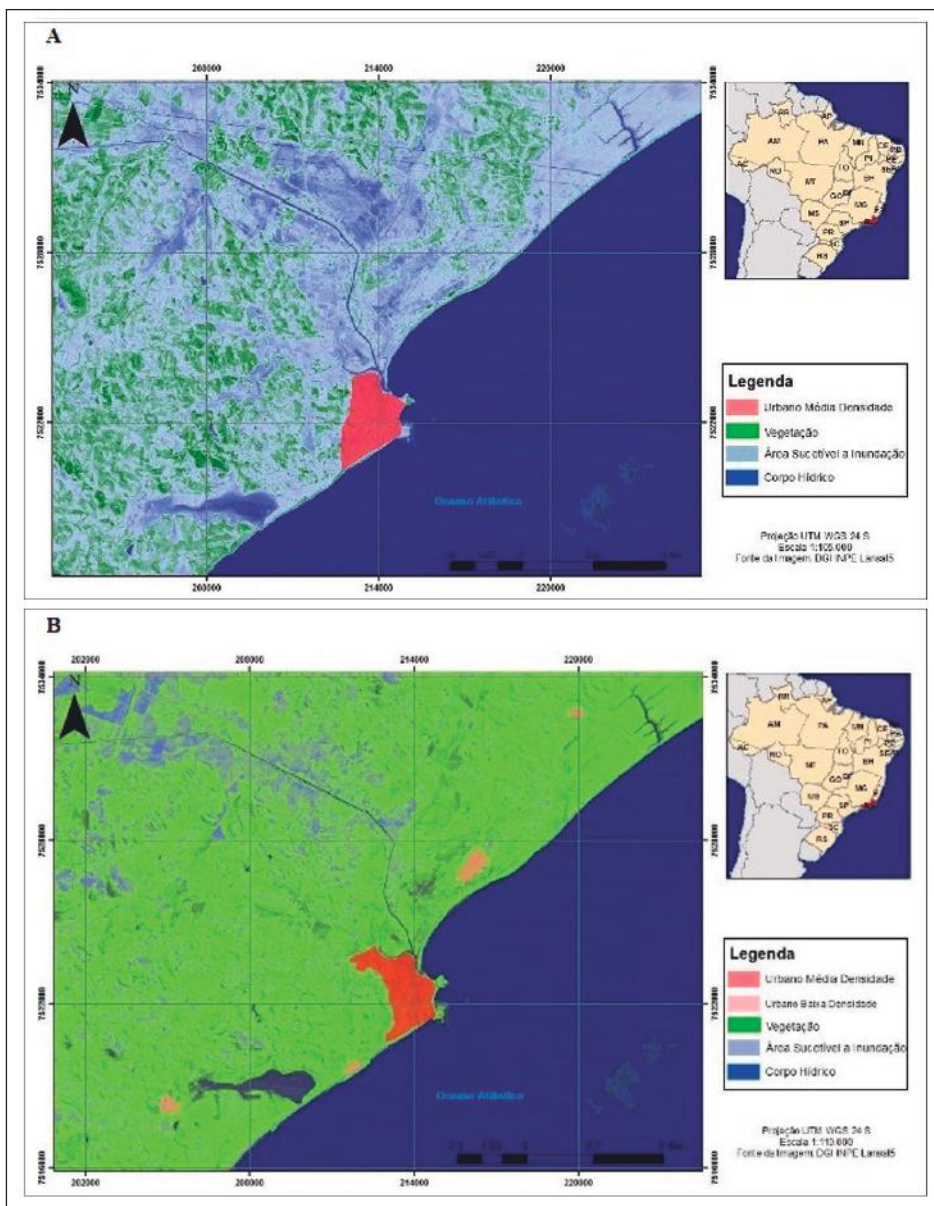
Figure 2: A. Land use and land cover representing the 1980s (image of 03/23/1985); B: 1990s (image of 07/30/1991).

river plain, which declined in the 2000s until small areas were identified in the year 2010. This decrease may be related to the expansion of the urban area of the city, (areas of ponds, swamps and river arms).

4.2. Seasonal and Time-Spatial Analysis of the Land Surface Temperature (LST)

In the seasonal analysis, the maps show a higher homogeneity of LST in dry (winter) than wet (summer) periods, in both years compared (2005 and 2010). In the summer (Figure 4A), due to the higher surface warming, the spectral responses varied, especially in the non-urbanized area. LST in the urban area varied between 30.1 and 32°C and the hottest areas. Temperature ranging between 34.1 and 38°C were identified in the central area and along the coastline (northbound). In the non-urban area, there is a predominance of temperatures between 26.1 and 28°C, but also with temperatures between 28.1 and 32°C. In winter (Figure 4B), as can be observed, the LST is very homogeneous in a large area and presented values much smaller in relation to the summer, values below 24°C. Some small spaces presented LST between 24.1 and 26°C, becoming urban areas.
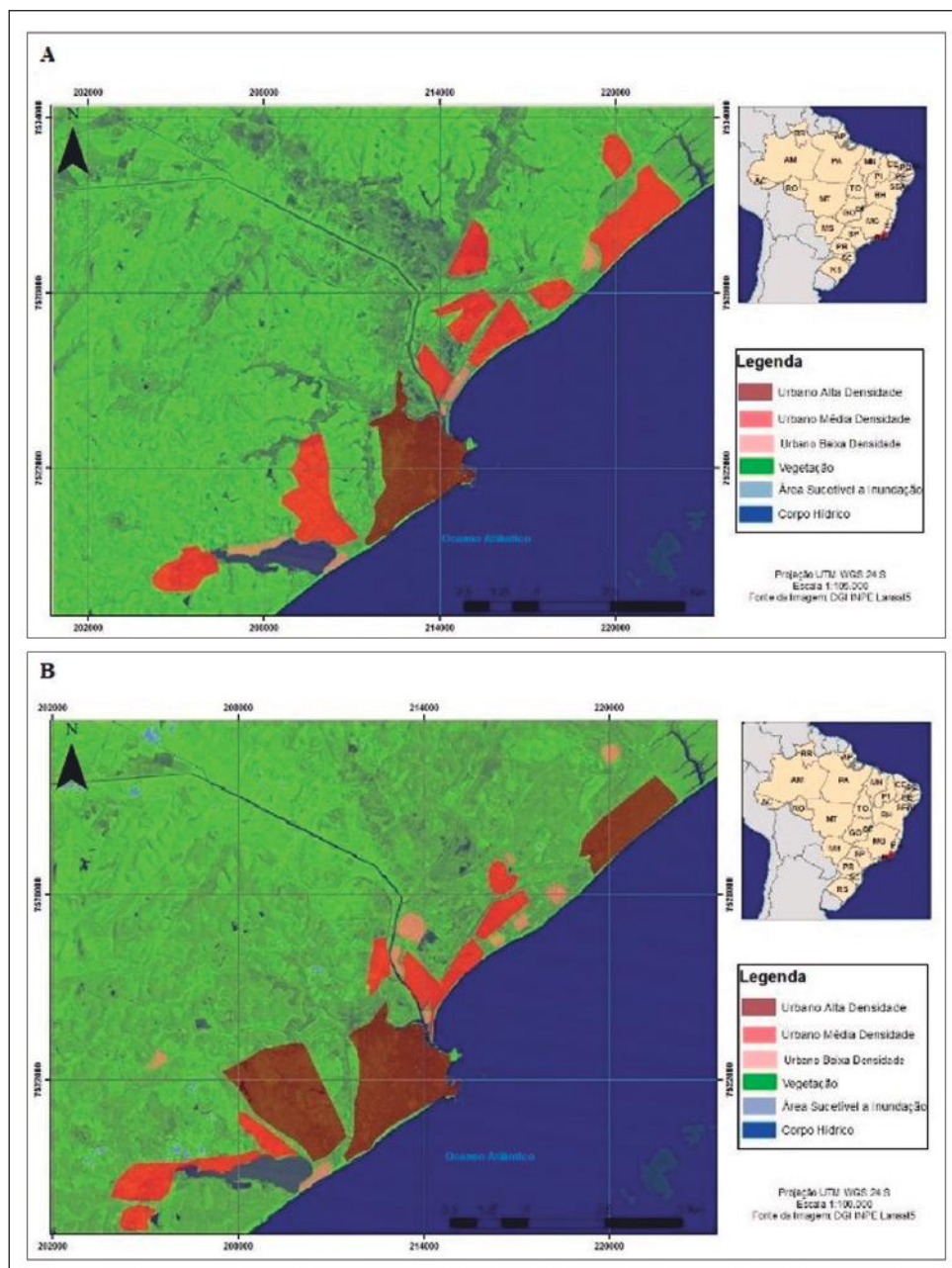
Figure 3 A: Land use and land cover representing the 2000's (image of 01/09/2005); B: 2010's (image of 03/23/2010).

In the image of the 01/09/2005 an area expansion with higher LSTs was observed, together with urban area expansion (as shown in the land use map). The values between 30.1 and 38°C became predominant in urban areas, once again showing the sensitivity of the central and northeast coast of Macaé. In the non-urban area, the predominant values were in the range between 26.1 and 30°C.

In the seasonal analysis of 2010, (Figure 5A) the highest summer temperatures in the urban area

can be identified with values between 30.1 and 34°C. Smaller, warmer cores show values up to 40°C. In the non-urban area, temperatures between 26.1 and 30°C predominated, although an area near the bed of the Macaé's river resulted in temperatures between 32.1 and 38°C. In the non-urban area temperatures were between 26.1 and 28°C, and in 2010 there was an expansion of the areas with temperatures between 28.1 and 30°C. There were also areas that showed up to 40°C. In urban areas, in 2005, there were more
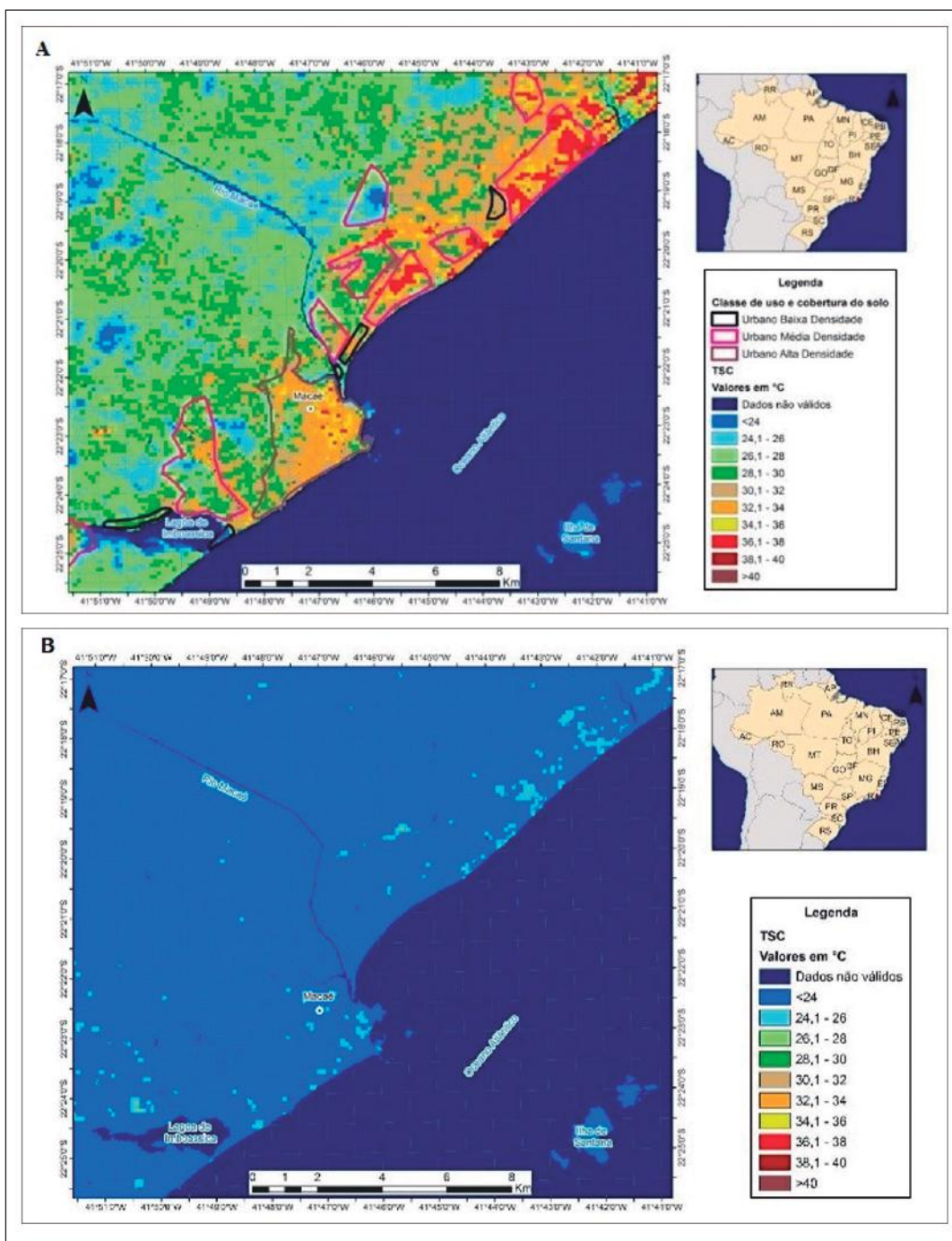
Figure 4 A: LST's map representing the 2000's summer (image of 01/09/2005); B: 2000's winter (image of 07/04/2005).

spaces with higher temperatures (between 36 and over 40°C) than in 2010, mainly in the urban area located on the north coast of the city. These areas can be evidenced as sites favorable to the formation of heat islands.

In winter (Figure 5B) the results showed that temperatures in 2005 are well below that in 2010, both in urban and non-urban areas. In 2010 the non-urban areas presented high values, above 40°C. This LST response greater than 40°C in winter may have relationships with other facts besides the surface. It is worth noting that between 2009 and 2010, the El Niño phenomenon of moderate intensity was recorded, and that such an event may influence the increase in air temperature in some regions of Brazil, as well as its influence on the atmospheric dynamics.
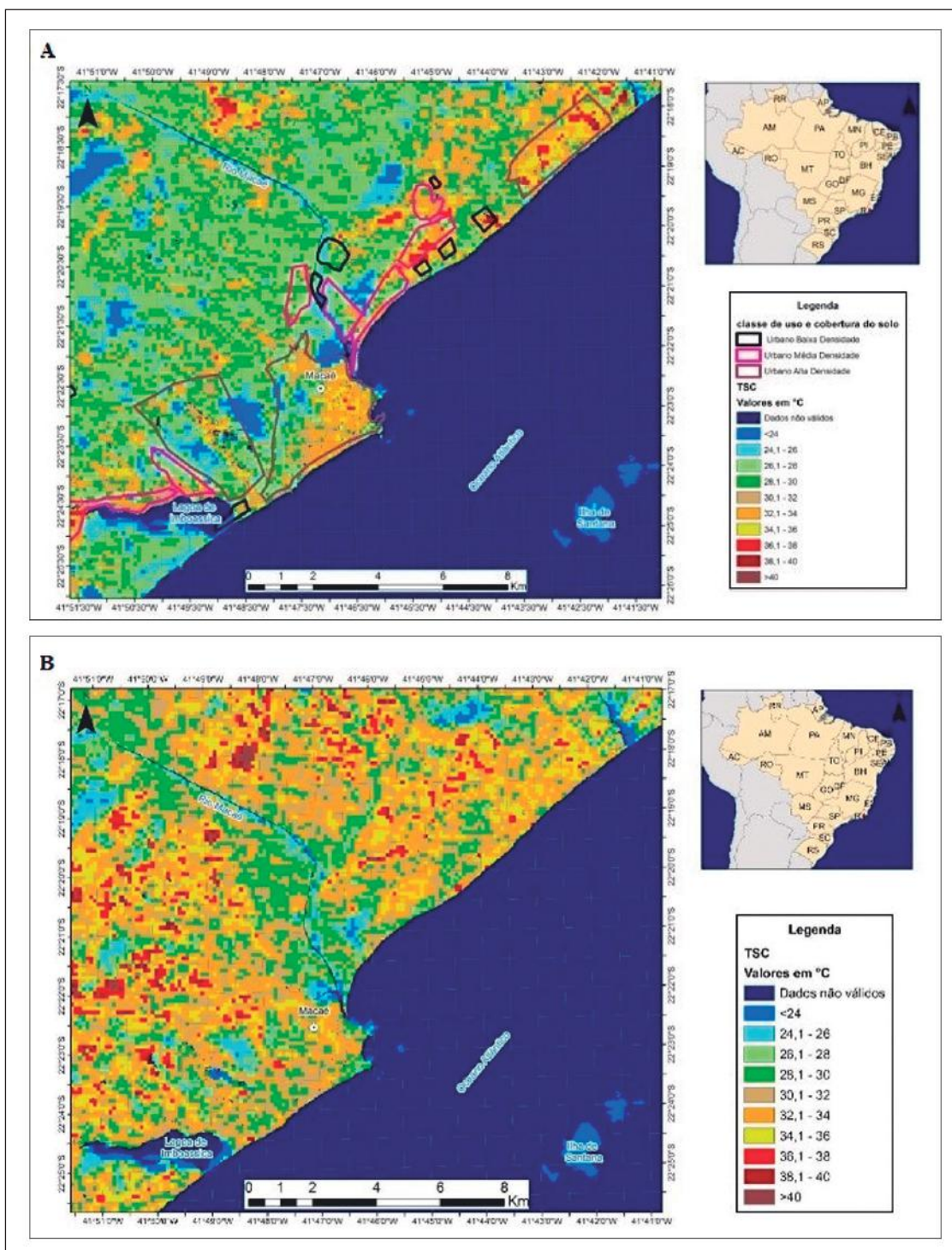
Figure 5 A: LST map representing the 2010's summer (image of 03/23/2010); B: 2010's winter (image of 09/04/2010).

Visually the 2010 winter thermal map is warmer than the summer thermal map. This fact is much more a situation of atmospheric order than the surface, that is to say, the atmospheric conditions of the episode of winter favored higher temperatures.

Also, the winter episode is in the month of September, which is the month that marks the beginning of spring in the southern hemisphere with a warmer atmosphere and trend of higher temperatures. On the other hand, the summer episode, at the end of March,

already limits with the beginning of autumn. In the image of the 03/23/2010, non-urban areas presented higher temperatures in comparison to 2005, and a retraction of the hottest areas in the urban region. The LST values that predominated in the urban area were in the range between 30.1 and 34°C, having surface points with temperatures between 36.1 and 40°C. In the non-urban area, the values between 26.1 and 30°C were predominant, and some points of the surface with temperatures between 32.1 and 40°C It was possible to observe that the highest LST values advanced in the urban areas.

The LST of the image of 03/23/1985 (Figure 6A) shows values between 32 and 36°C, and between 36 and 40°C in the central urban area and the city's coast. In non-urban areas, values predominated between 28 and 32°C. The winter image presented on July 30, 1991 (Figure 6B) presented lower LSTs with little variation between urban and non-urban areas. The values between 26 and 28° C predominated in the urban area, and between 28 and 30°C in the non-urban area. Some spaces presented temperatures between 24.1 and 26°C, and below 24°C, mainly in the areas near the Macaé river and areas with more dense vegetation cover.

4.3. Time-Spatial Analysis of the NDVI

In the image of 03/23/1985 (Figure 7A) NDVI values were between 0.1 and 0.45 in most of the urban area, representing low composition of the vegetable mass. In the non-urban area, the predominant value is between 0.45 and 0.75, corresponding to the area with more consistent and dense vegetation cover. Even in the non-urban area, considered as "vegetation", it was possible to observe spaces that presented values between 0.1 and 0.45, which may be related to specific soil and vegetation characteristics (these characteristics were not detailed in the present study), thus, the spectral response was not the same for any area considered as vegetation.

In the image of July 30, 1991 (Figure 7B), the prevalence of values between 0.1 and 0.3, and between 0.3 and 0.45, in the urban area, as well as in several Urban areas. It is worth mentioning that the image is of a winter episode, and the vegetation cover may present changes in its physical characteristics due to the humidity, in this case, the possibility is of

a drier vegetation. In this image, it is already possible to see a decrease of the vegetated areas, due to the growth of the city of Macaé, mainly in the coastal coast and in the central region of the city.

In the results of the image of 01/09/2005 (Figure 8A), the increase of areas with values between 0.1 and 0.45 (represented in orange and yellow tones on the map) is perceptible, and, at the same time, an increase of urban area. That is, the advance of the urban area generating values below zero and corresponding to the low composition of vegetable mass. In the non-urban area values between 0.45 and 0.75 were predominant, which responds well to a healthy vegetation cover area. It was also possible to observe non-urban areas that presented values between 0.3 and 0.45, mainly in the vicinity of the bed of the Macaé's river - area susceptible to flooding, and on the north coast of Macaé - an area that shows remnants of sandy cords and restinga.

In the image of 03/23/2010 (Figure 8B), the NDVI values that predominated in the urban area were between 0.1 and 0.15. The urban area expanded little in relation to the image of 2005, but there was an increase of urban area around the Imboassica Lagoon. In the vicinity of the Macaé's river, values close to 0.1 and 0.15 intensified, also showing an advance of the urban area and a change in the area susceptible to flooding. The non-urban area presented alterations in the spectral response, and more spaces with values between 0.3 and 0.45 were identified, showing low vegetation composition in these areas.

Among the four analyzed images, the greatest difference could be identified between 1990 and 2000 (07/30/1991 and 01/09/2005, respectively), where it was possible to observe, together with the analysis of land use change, which was the most significant growth of the urban area. The NDVI results were practically the same as those of the LST, where the highest values of NDVI (close to 1) crossed with the lowest values of LST, showing the difference in the spectral response of the most vegetated areas and less vegetated.

5. Conclusions

The analysis made through the satellite images indicate that the urban space of Macaé is favorable to the occurrence of heat islands, and that, however
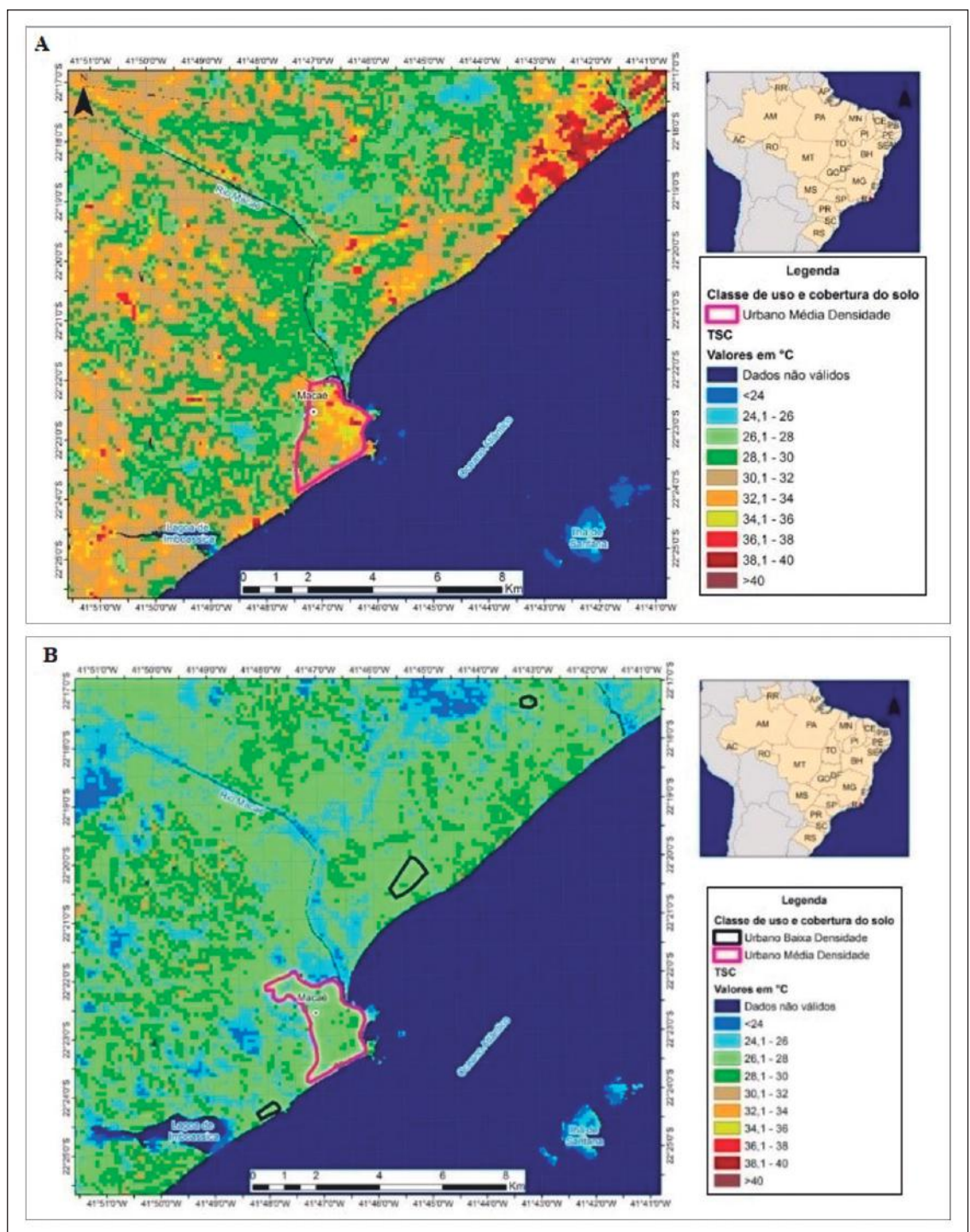
Figure 6 A: LST map representing the 1980's summer (image of 03/23/1985); B: 1990's winter (image of 07/30/1991).

minor the change in the use and occupation of the soil, changes in the LST can be perceived. Most of the municipality of Macaé is not urbanized, but with different particularities in its coverage, reflecting in its spectral responses similarly for all indexes used in this work.

The results showed an approximation of the LST with the use and coverage of the soil, mainly in the images that represent the years 2000 and 2010. The highest values of LST in the urban area corresponded to values closer to -1 (for NDVI), indicating area Less vegetated, that is, the two parameters crossed.
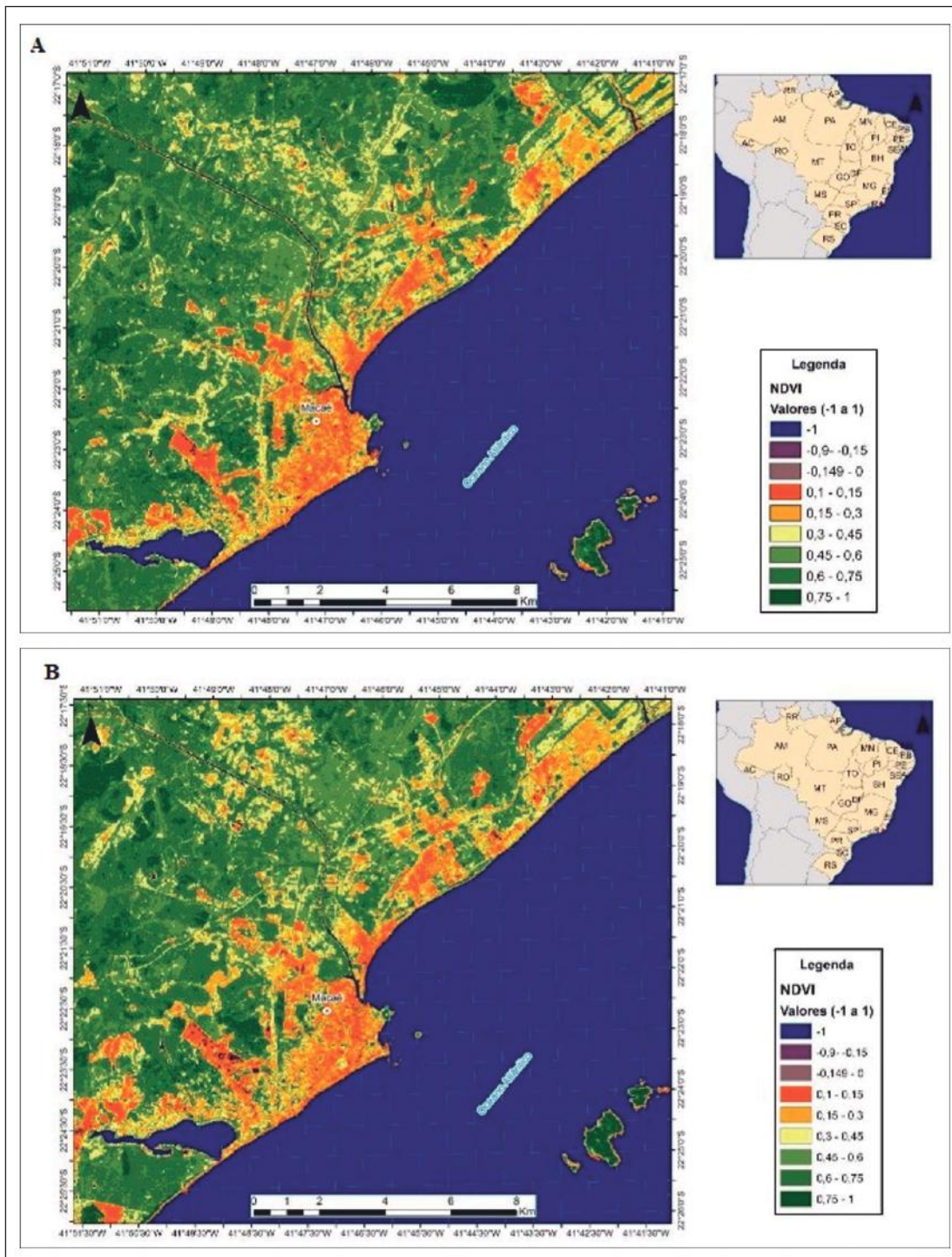
Figure 7 A: NDVI map representing the 1980's summer (image of 03/23/1985); B: 1990's (image of 07/30/1991).

Likewise, for the non-urban areas the highest LSTs corresponded to the values closest to -1 (for NDVI).

The best response for the expansion of the urban area in front of the analyzed images was obtained through the NDVI, because the retraction of vegetated areas was more noticeable than the variation of LST (in time and space). Soil use and cover presented a good approximation with LST and NDVI, main-
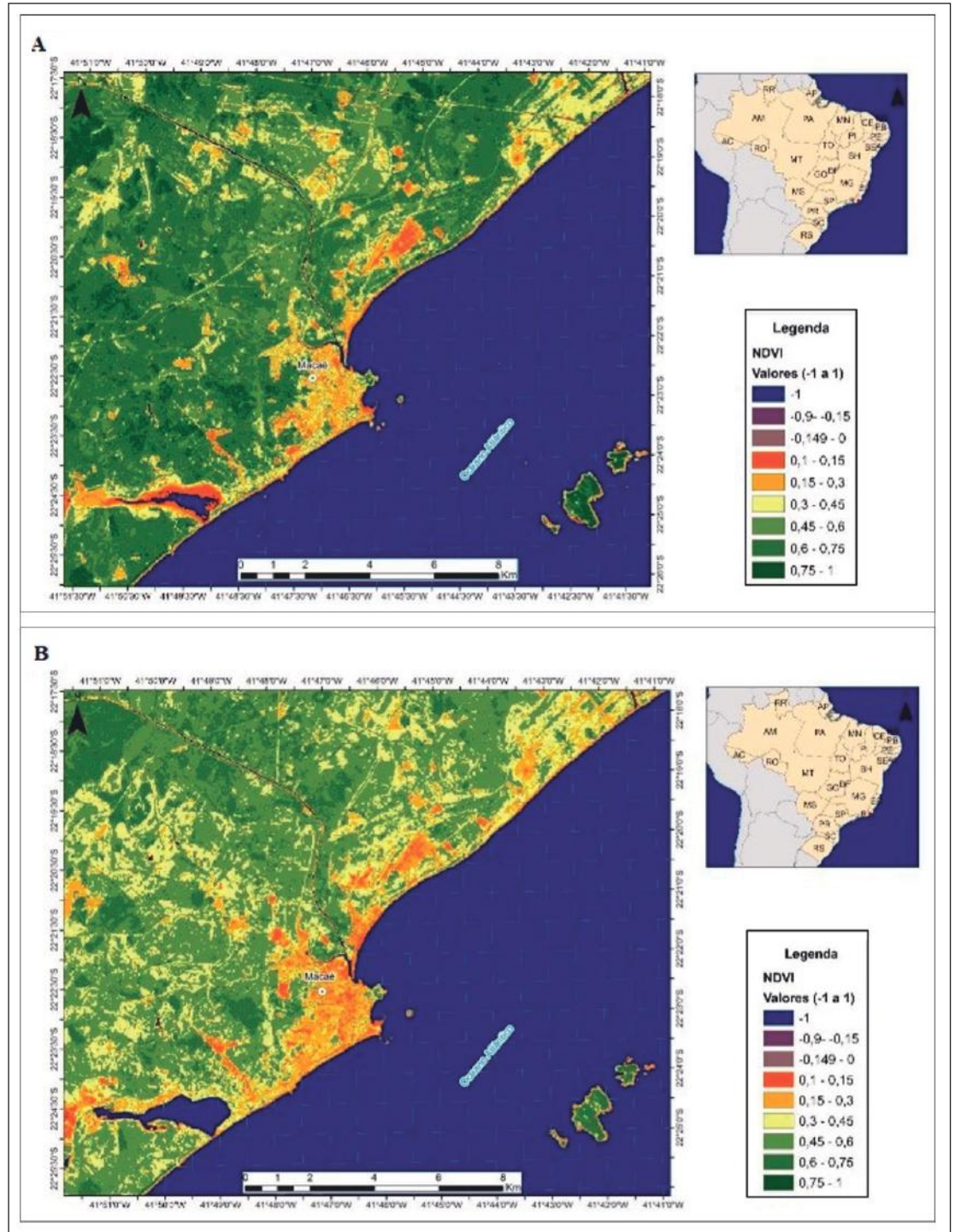
Figure 8 A. NDVI map representing the 2000's (image of 01/09/2005); B. NDVI map of the 03/23/2010 representing the decade of 2010.

ly for urban areas. This is because non-urban areas have been classified with only one class of "vegetation", which may have masked / concealed the different ways in which the vegetation, and all its diversity of colors and shapes, gives its spectral response.

The satellite images also presented a limiting framework for this work, since almost all of the images covered clouds and noise, making it even more difficult to make new results. With this, the performance of statistical tests.

The mapping of urban land use and land cover through vectored polygons was very useful to demonstrate the hottest areas identified in the most urbanized areas. The urbanized area of Macaé is considered small, which facilitated in the manual vectorization allowing a satisfactory result, mainly when compared with satellite images of Google Earth.

In the mapping of land use and land cover it was possible to identify a change in the geographic space and to realize that the study area presents much more peculiarities than expected, bringing reflections and new inquiries about the environmental characteristics of the region.

The oil industry was installed in Macaé from the 70's, and brought with it new forms for the city. Such forms as the creation of circulation routes, building lots and neighborhoods and a whole network of services to meet the demand and needs of this industry. in addition, these forms helped leverage the economy of the city. The population of Macaé grew from 74,000 inhabitants in 1974 to 206,728,000 in 2010. However, due to the current oil and economic crisis in the state of Rio de Janeiro, a new demographic and urban pattern should be designed in the coming years. Recent discoveries in the Campos Basin are underway.

6 References

Allen, R.; Tasumi, M. & Trezza, R. 2002. SEBAL (Surface Energy Balance Algorithms for Land)-Advanced Training and User's Manual-Idaho Implementation, Version 1.0, 97p.

Bastiaanssen, W.G.M., 2000.SEBAL-Based Sensible and Latent Heat Fuxes in the Irrigated Gediz Basin, Turkey. *Journal of Hydrology*, 229: 87–100.

Buyantuyev, A. & Wu, J. 2010. Urban Heat Islands and Lands-Cape Heterogeneity: Linking Spatiotemporal Variations in Surface Temperatures to Land - Cover and Socioeconomic Patterns. *Landscape Ecology*, 25: 17-33.

Carlson, T.N.; Augustine, J.N. & Boland, F.E. 1977. Potential Application of Satellite Temperature Measurements in the Analysis of Land Use over Urban Areas. *Bulletin of the American Meteorological Society*, 58: 1301-1303.

Chander, G. & Markham, B.L. 2003. Revised Landsat-5 TM Radiometric Calibration Procedures, and Post-Calibration Dynamic Ranges. *IEEE Transactions on Geoscience and Remote Sensing*, 41: 2674−2677.

Chander, G.; Markham, B.L. & Helder, D.L. 2009. Summary of Current Radiometric Calibration Coefficients for Landsat MSS, TM, ETM+, and EO-1 ALI Sensors. *Remote Sensing of Environment*, *113*: 893-903.

Chen, Z.; Gong, C.; Wu, J. & Yu, S. 2012. The Influence of Socioeconomic and Topographic Factors on Nocturnal Urban Heat Islands: a Case Study in Shenzhen, China. *International Journal of Remote Sensing*, 33 (12): 3834-3849.

Cheval, S.; Dumitrescu, A. & Bell, A. 2009. The Urban Heat Island of Bucharest during Extreme Hight Temperature of July 2007. *Theoretical and Applied Climatology*, 97: 391-401.

França, G.B.& Cracknell, A.P.A. 1995.Simple cloud masking approach using NOAA AVHRR daytime data for tropical areas. *International Journal of Remote Sensing*, 16(9): 1697–1705.

Huete, A.; Didan, K.; Miura, T.; Rodriguez, E.P.; Gao, X. & Ferreira, L.G. 2002. Overview of the Radiometric and Biophysical Performance of the MODIS Vegetation Indices. *Remote Sensing of Environment*, *83*: 195-213.

IBGE – Instituto Brasileiro de Geografia e Estatística. Censo demográfico 2010: Available in http://cidades.ibge.gov.br/xtras/temas.php?lang=&codmun=330240&idtema=1&search=rio-de-janeiro/macae/censo-demografico-2010:-sinopse. Accessed Jul 137, 2019.

Iqbal, M. 1983. *An Introduction to Solar Radiation*. Ontario, Canadian Academic Press. 389 p.

Julien, Y., Sobrino, J.A. & Verhoef, W., 2006. Changes in land surface temperatures and NDVI values over Europe between 1982 and 1999. *Remote Sensing of Environment*, 103: 43–55;

Leal, G.C.S. G; Farias, M.S.S. & Araújo, A.F. 2008. O Processo de Industrialização e seus Impactos no Meio Ambiente Urbano. *QUALIT@S Revista Eletrônica*. 7: 1-11.

Li, J.; Song, C.; Cao, L.; Zhu, F.; Meng, X. & Wu, J. 2011. Impacts of Landscape Structure on Surface Urban Heat Islands: A Case Study of Shanghai, China. *Remote Sensing of Environment*, *115*: 3249–3263.

Lucena, A.J.; Rotunno Filho,O. C.; França, J.R.A.; Peres, L.F. & Xavier, L.N.R. 2013. Urban Climate and Clues of Heat Island Events in the Metropolitan Area of Rio de Janeiro. *Theoretical Applied Climatology*, *111*: 497-511.

Marques, M. A. 2008. *Qualidade de Vida no Município de Macaé-RJ: Análise por Geoprocessamento*. Programa de Pós-graduação em Geografia, Universidade Federal do Rio de Janeiro, Tese de Doutorado, 300p.

Matson, M.; Mcclain, E.P.; Mcginnis, D.F.Jr. & Pritchard, J.A. 1978. Satellite Detection of Urban Heat Islands. *Monthly Weather Review*, *106*: 1725-1734.

Sena, C.A.P..; França, J.R.A. & Peres, L.F. 2014. Estudo da Ilha de Calor na Região Metropolitana do Rio de Janeiro Usando Dados do MODIS. *Anuário do Instituto de Geociências, 37* (2): 111-122.

Oke, T. R. 1987. *Boundary Layer Climate* (2nd end). London, Routledge. 435p.

Peres, L.F.; Lucena, A.J.; Rotunno Filho, O.C. & França, J.R.A. 2018. The Urban Heat Island in Rio de Janeiro, Brazil, in the Last 30 Years Using Remote Sensing Data. *International Journal of Applied Earth Observation and Geoinformation*, *64*: 104-116.

Ponzoni, F.J. & Shimabukuro, Y.E. 2007. *Sensoriamento Remoto no Estudo da Vegetação*. São José dos Campos-SP,

Parêntese. 127p.

Qin, Z.; Karnieli A. & Berliner P. 2001. A Mono-Window Algorithm for Retrieving Land Surface Temperature from Landsat TM Data and Its Application to the Israel-Egypt Border Region. *International Journal of Remote Sensing*, *22* (18): 3719–3746.

Rao, P. K. 1972. Remote Sensing of Urban Heat Islands from an Environmental Satellite. *Bulletin of the American Meteorological Society*, *53*: 647– 648.

Rhinane, H.; Hilali, A.; Bahi, H. & Berrada, A. 2012. Contribution of Landsat TM Data for the Detection of Urban Heat Islands Areas Case of Casablanca. *Journal of Geographic Information System*, *4*: 20-26.

Sena, C.A.P.; França, J.R.A. & Peres, L.F. 2014. Um Estudo do Fenômeno da Ilha de Calor Urbana na Região Metropolitana do Rio de Janeiro (RMRJ). *Anuário do Instituto de Geociências, 37* (2): 180-194.

Sobrino, J.A.; Oltra-Carrió, R.; Jiménez-Muñoz, J.C.; Julien, Y.; Sòria, G.; Franch, B. & Matta, C. 2012. Emissivity Mapping over Urban Areas Using a Classification-Based Approach: Application to the Dual-Use European Security IR Experiment (DESIREX). *International Journal of Applied Earth Observation and Geoinformation*, *18*: 141–147.

Souza, J. D. & Silva, B. B. 2005. Correção Atmosférica para Temperatura da Superfície Obtida com Imagem de Landsat 5. *Revista Brasileira de Geofísica*, *23* (4): 349-358.